

# Electromagnetic calorimeters based on scintillating lead tungstate crystals for experiments at Jefferson Lab <sup>☆</sup>

A.Asaturyan<sup>a</sup>, F.Barbosa<sup>c</sup>, V.Berdnikov<sup>b</sup>, J.Crafts<sup>g</sup>, H.Egiyan<sup>c</sup>, L.Gan<sup>f</sup>, A.Gasparian<sup>g</sup>, K.Harding<sup>c</sup>, T.Horn<sup>b</sup>, V.Kakoyan<sup>a</sup>, H.Mkrtchyan<sup>a</sup>, Z.Papandreou<sup>e</sup>, V. Popov<sup>c</sup>, S.Taylor<sup>c</sup>, N.Sandoval<sup>c</sup>, A.Somov<sup>c,\*</sup>, S.Somov<sup>d</sup>, A. Smith<sup>h</sup>, C. Stanislav<sup>c</sup>, H. Voskanyan<sup>a</sup>, T. Whitlatch<sup>c</sup>, S. Worthington<sup>c</sup>

<sup>a</sup>A. I. Alikhanian National Science Laboratory (Yerevan Physics Institute), 0036 Yerevan, Armenia

<sup>b</sup>Catholic University of America, Washington, DC 20064, USA

<sup>c</sup>Thomas Jefferson National Accelerator Facility, Newport News, VA 23606, USA

<sup>d</sup>National Research Nuclear University MEPhI, Moscow, Russia

<sup>e</sup>University of Regina, Regina, Saskatchewan, Canada S4S 0A2

<sup>f</sup>University of North Carolina at Wilmington, Wilmington, NC 28403, USA

<sup>g</sup>North Carolina A&T State University, Greensboro, NC 27411, USA

<sup>h</sup>Duke University, Durham, North Carolina 27708, USA

## Abstract

A new electromagnetic calorimeter consisting of 140 lead tungstate (PbWO<sub>4</sub>) scintillating crystals was constructed for the PrimEx  $\eta$  experiment at Jefferson lab. The calorimeter was integrated into the DAQ and trigger systems of the GlueX detector and used in the experiment to reconstruct Compton scattering events. The experiment started collecting data in the spring of 2019 and acquired about 30% of the required statistics. The calorimeter is a prototype for two PbWO<sub>4</sub>-based detectors, which are currently under construction at Jefferson Lab: the Neutral Particle Spectrometer (NPS) and the lead tungstate insert of the forward calorimeter (FCAL) of the GlueX detector. The article presents the design and performance of the Compton calorimeter and gives a brief overview of the FCAL and NPS projects.

**Keywords:** Electromagnetic calorimeter, Lead tungstate scintillator

## 1. Introduction

Electromagnetic calorimeters based on PbWO<sub>4</sub> scintillating crystals have a widespread application in experiments at different accelerator facilities such as CERN, FNAL, GSI, and Jefferson Lab (JLab). The small radiation length ( $L_R = 0.89$  cm) and Molière radius ( $R_m = 2.19$  cm) of PbWO<sub>4</sub> allows to build high-granularity detectors with a good spatial separation and energy resolution of reconstructed electromagnetic showers, which makes these crystals the material of choice in many of these applications.

Two electromagnetic calorimeters are currently under construction in experimental Hall D and Hall C at Jefferson Lab, both using 2.05 cm x 2.05 cm x 20 cm PbWO<sub>4</sub> scintillating modules. The inner part of the forward lead glass calorimeter of the GlueX detector [1] in Hall D will be upgraded with these high-granularity, high-resolution crystals. This upgrade is required by the physics program with the GlueX detector, specifically the new experiment to study rare decays of  $\eta$  mesons [2]. The size of the insert will tentatively consist of

2496 lead tungstate modules. The Neutral Particle Spectrometer [3] in experimental Hall C consists of a PbWO<sub>4</sub> electromagnetic calorimeter preceded by a sweeping magnet. The NPS is required by Hall C's precision cross section measurement program with neutral final states [4–9]. Such precision measurements of small cross sections play a central role in studies of transverse spatial and momentum hadron structure. The NPS detector consists of 1080 PbWO<sub>4</sub> crystals arranged in a 30x36 array. Lead tungstate crystals for both detectors were procured from two vendors: Shanghai Institute of Ceramics (SICCAS) in China and CRYTUR in the Czech Republic. The quality of recently produced PbWO<sub>4</sub> scintillators has been studied in detail by the NPS and EIC eRD1 collaborations and is described in Ref. [10]. PbWO<sub>4</sub> crystals are also being considered for an electromagnetic calorimeter of the future Electron-Ion Collider [11].

In this article we describe the design and construction of a calorimeter prototype composed of 140 SICCAS crystals, which served as the Compton Calorimeter (CCAL) in the PrimEx  $\eta$  experiment [12] with the GlueX detector in the spring of 2019. The CCAL was subsequently used during a few short GlueX physics runs at high luminosity in order to study rates and operating conditions expected for the FCAL lead-tungstate insert. Experience gained during fabrication and operation of the CCAL was critical for finalizing the design of the FCAL insert and also helped further optimize the NPS calorimeter.

<sup>☆</sup>Notice: Authored by Jefferson Science Associates, LLC under U.S. DOE Contract No. DE-AC05-06OR23177. The U.S. Government retains a non-exclusive, paid-up, irrevocable, world-wide license to publish or reproduce this manuscript for U.S. Government purposes.

\*Corresponding author. Tel.: +1 757 269 5553; fax: +1 757 269 6331.

Email address: somov@jlab.org (A.Somov)

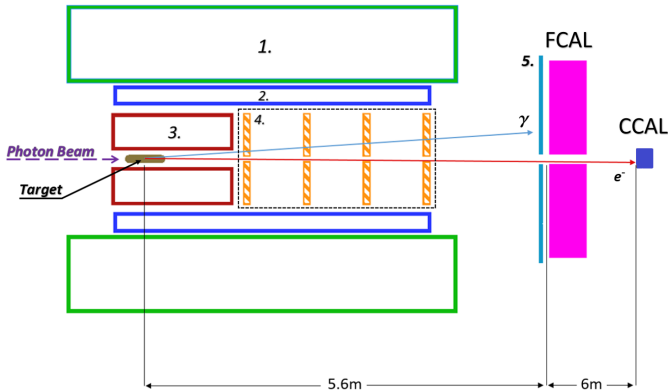


Figure 1: Schematic layout of the GlueX detector (not to scale). Numbers represent the following detector components: solenoid magnet (1), barrel calorimeter (2), central drift chamber (3), forward drift chambers (4), time-of-flight wall (5).

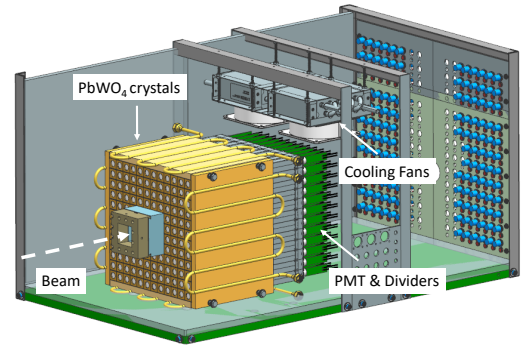


Figure 2: Schematic layout of the Compton calorimeter.

This article is organized as follows: we will present the PrimEx  $\eta$  experiment and performance of the CCAL in Section 2 and Section 3, and will briefly describe the FCAL and NPS projects in Sections 4 and 5.

## 2. PrimEx $\eta$ experiment with the GlueX detector

The GlueX detector [1] was designed to perform experiments using a photon beam. Beam photons are produced via the bremsstrahlung process by electrons, provided by the JLab electron accelerator facility, incident on a thin radiator. The energy of a beam photon is determined by detecting a scattered electron using tagging scintillator detectors with a typical precision of 0.2%.

The physics goal of the PrimEx  $\eta$  experiment is to perform a precision measurement of the  $\eta \rightarrow \gamma\gamma$  decay width. The measurement will provide an important test of QCD symmetries and is essential for the determination of fundamental properties such as the ratios of the light quark masses and the  $\eta$ - $\eta'$  mixing angle. The decay width will be extracted from the measurement of the photoproduction cross section of  $\eta$  mesons in the Coulomb field of a nucleus, which is known as the Primakoff effect.  $\eta$  mesons will be reconstructed by detecting two decay photons in the forward calorimeter of the GlueX detector.

The cross section will be normalized using the Compton process, which will also be used to monitor the luminosity and control the detector stability during data taking. Electrons and photons originating from Compton events in the target are produced at small angles, typically outside the acceptance of the FCAL. In order to improve the reconstruction of particles in the forward direction, we built a small Compton calorimeter consisting of 140 lead tungstate scintillating crystals and positioned it about 6 m downstream from the FCAL. The CCAL covers the angular range between  $0.18^\circ$  and  $0.33^\circ$ . A schematic view of the GlueX detector and the position of the Compton calorimeter is illustrated in Fig. 1.

The PrimEx  $\eta$  experiment started collecting data in the spring of 2019 and has acquired 30% of the required statistics. During the experiment, the magnetic field of the solenoid magnet was switched off in order to allow reconstruction of Compton events. The photon flux was about  $5 \cdot 10^6 \gamma/\text{sec}$  (four times lower than the nominal GlueX flux) in the beam energy range of interest between 9.5 GeV and 11.6 GeV.

## 3. Compton calorimeter of the PrimEx $\eta$ experiment

### 3.1. Calorimeter design

The calorimeter design is shown in Fig. 2. The CCAL is comprised of an array of 12 x 12 lead tungstate modules with a 2 x 2 hole in the middle for the passage of the photon beam. The modules are positioned inside a light tight box. A tungsten absorber is placed in front of the innermost layer closest to the beamline to provide protection from the high rate of particles predominantly originating from electromagnetic interactions.

The light yield from PbWO<sub>4</sub> crystals depends on temperature with a typical temperature coefficient of 2%/°C at room temperature. Maintaining constant temperature is essential for the calorimeter operation. Calorimeter modules are surrounded by four copper plates with built-in pipes to circulate a cooling liquid and provide temperature stabilization. Foam insulation surrounded the detector box. The temperature was monitored and recorded during the experiment by five thermocouples attached to different points of the PbWO<sub>4</sub> module assembly. During the experiment the temperature was maintained at  $17^\circ \pm 0.2^\circ\text{C}$ . The typical heat released by the photomultiplier tube (PMT) dividers was equivalent to 33 Watts. In order to prevent condensation, a nitrogen purge was applied. Two fans with the water-based cooling system were installed on the top of the crystal assembly to improve nitrogen circulation and heat dissipation from the PMT dividers. The detector was positioned on a movable platform, which provided motion in the vertical and horizontal directions, perpendicular to the beam. The platform was remotely controlled and provided a position accuracy of about 200  $\mu\text{m}$ . During detector calibration each module was moved into the beam.

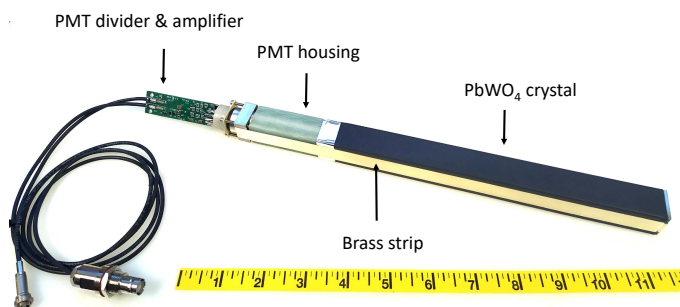


Figure 3: Calorimeter module showing all components: the PbWO<sub>4</sub> crystal, PMT housing, PMT divider, and signal and HV cables.

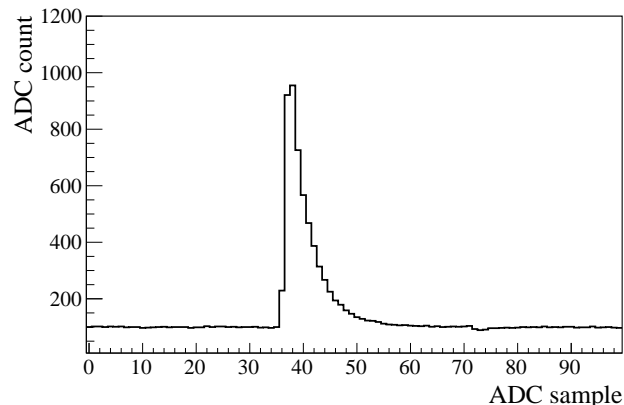


Figure 4: A typical flash ADC signal pulse obtained from a PbWO<sub>4</sub> module.

### 3.2. Module design

The design of the PbWO<sub>4</sub> module is based on the HyCal calorimeter, which was used in several experiments in Jefferson Lab Hall B [13]. An assembled calorimeter module is presented in Fig. 3. Each lead tungstate crystal is wrapped with a 60  $\mu\text{m}$  polymer Enhanced Specular Reflector film (ESR) manufactured by 3M<sup>TM</sup>, which allows 98.5% reflectivity across the visible spectrum. In order to improve optical isolation of each module from its neighbors, each crystal was wrapped with a layer of 25  $\mu\text{m}$  thick Tedlar. The PMT is located inside a G-10 fiberglass housing at the rear end of the crystal. Two flanges are positioned at the crystal and housing ends and are connected together using 25  $\mu\text{m}$  brass straps, which are brazed to the sides of the flanges. Four set screws are pressed to the PMT housing flange to generate tension in the straps and hold the assembly together. Light from the crystal is detected using a ten-stage Hamamatsu PMT 4125, which is inserted into the housing and is coupled to the crystal using optical grease (BC-631). The PMT diameter is 19 mm. The PMT is pushed towards the crystal by using a G-10 retaining plate attached to the back of the PMT and four tension screws applied to the PMT flange. The PMT is instrumented with a high-voltage divider and amplifier positioned on the same printed circuit board attached to the PMT socket.

### 3.3. Electronics

The PMT of each calorimeter module was equipped with an active base prototype [14], which was designed for the Neutral Particle Spectrometer in experimental Hall C. The base combines a voltage divider and an amplifier powered by the current flowing through the divider. The active base allows the operation of the PMT at lower voltage and consequently at lower anode current, which improves the detector rate capability and prolongs the PMT's life. The original Hamamatsu divider for this type of PMT was modified by adding two bipolar transistors on the last two dynodes, which provides gain stabilization at high rate. The active base from the NPS detector has a relatively large amplification of about a factor of 24 due to the large PMT count rate predicted by Monte Carlo simulation. Large amplification was not needed for the planned run conditions for the

PrimEx  $\eta$  experiment. However, we subsequently used CCAL in GlueX runs at significantly larger luminosity in order to study run conditions of the FCAL lead tungstate insert, where the amplifier will be required. This will be discussed in Section 4.0.3. During the PrimEx run, the CCAL was operated at about 680 V, which produced a divider current of 260  $\mu\text{A}$ . The high voltage for each PMT was supplied by a 24-channel CAEN A7236SN module positioned in a SY4527 mainframe.

Amplified PMT signals were digitized using a twelve-bit 16-channel flash ADCs electronics module operated at a sampling rate of 250 MHz. The ADC was designed at Jefferson Lab [15] and is used for the readout of several sub-detectors of the GlueX detector. The Field-Programmable Gate Array (FPGA) chip inside the ADC module allows the implementation of various programmable data processing algorithms for the trigger and readout. An example of a flash ADC signal pulse obtained from a calorimeter module is shown in Fig. 4. In this example, the ADC is operated in the raw readout mode, where digitized amplitudes are read out for 100 samples, corresponding to the 400 ns read out window. During the PrimEx  $\eta$  experiment, the ADC performed on-board integration of signal pulses, for amplitudes above a threshold of 24 MeV. ADC amplitudes are summed in a time window of 64 ns and reported by the ADC along with other parameters such as the pulse amplitude, pulse time, amplitude of the ADC pedestal, and data processing quality factors. This readout mode allowed to significantly reduce the data size and ADC readout time, and therefore did not induce any dead time in the DAQ.

CCAL flash ADCs are positioned in a VXS (ANSI/VITA 41.0 standard) crate. VXS crates are used to host all readout electronics of the GlueX experiment. In addition to the VME-bus used to read out data from electronics modules, the VXS is instrumented with a high-speed serial bus in order to increase the bandwidth to several Gb/sec and provide an interconnected network between modules. The bus is used to transmit amplitudes digitized by the ADC to trigger electronics modules and include the CCAL to the Level 1 trigger system of the GlueX detector.

194 **3.4. Light Monitoring System**

195 To monitor performance of each calorimeter channel, we  
 196 designed an LED-based light monitoring system (LMS). The  
 197 LMS optics includes a blue LED, a spherical lens to correct  
 198 the conical dispersion of the LED, and a diffusion grating to  
 199 homogeneously mix the light. Light produced by the LED is  
 200 incident on a bundle of plastic optical fibers (Edmund Optics)  
 201 with a core diameter of 250  $\mu\text{m}$ . Each fiber distributes light to  
 202 an individual calorimeter module. On the crystal end, the fiber  
 203 is attached to the module using a small acrylic cap glued to the  
 204 crystal with a hole drilled through each cap to hold the fiber  
 205 inside.

206 To monitor stability of the LED, we used two reference  
 207 Hamamatsu 4125 PMTs, the same type as in the CCAL detector.  
 208 Each PMT receives light from two sources: a single fiber  
 209 from the LED and a YAP:Ce pulser unit, both glued to the PMT  
 210 face. The pulser unit consists of a 0.15 mm thick YAP:Ce scin-  
 211 tillation crystal with a diameter of 3 mm spot activated by an  
 212  $^{241}\text{Am}$   $\alpha$  source. The  $\alpha$  source is used to monitor stability of  
 213 the LED. The PMT was read out using a flash ADC. The high  
 214 voltage on each reference PMT was adjusted to have the signals  
 215 from both the LED and  $\alpha$  source fit within the flash ADC range  
 216 of 4096 counts, as shown in Fig. 5. Each LED was driven by  
 217 a CAEN 1495 module, which allowed to generate LED pulses  
 218 with a programmable rate. The LMS was integrated into the  
 219 GlueX trigger system and provided a special trigger type during  
 220 data taking. The LMS was extensively used during the detector  
 221 commissioning and injected light to the CCAL detector with a  
 222 typical frequency of 100 Hz continuously during the PrimEx  $\eta$   
 223 experiment. This LED rate is similar to the trigger rate of events  
 224 generated by the reference  $\alpha$  source.

225 Most LMS components were positioned inside the  
 226 temperature-stabilized detector box. The stability of the  
 227 LED system measured using the reference PMTs during the  
 228 entire PrimEx run was better than 1%. The ratio of signal ADC  
 229 amplitudes from the LED pulser to the  $\alpha$  alpha source obtained  
 230 during different run periods of the 48-day long PrimEx  $\eta$   
 231 experiment is presented in Fig. 6. The ratio is normalized  
 232 to the data in the beginning of the experiment. Stability of  
 233 most CCAL modules observed using the LMS during the  
 234 experiment was better than 6%. We did not apply any PMT  
 235 gain adjustments during the experiment.

236 **3.5. Calibration**

237 The initial energy calibration of the CCAL was performed by  
 238 moving each calorimeter module into the photon beam during  
 239 special low-intensity calibration runs. The maximum rate in  
 240 the module, for a threshold of 15 MeV, did not exceed 200 kHz.  
 241 The energy of each beam photon was determined by detecting  
 242 a bremsstrahlung electron using the GlueX tagging detectors  
 243 described in Section 2. The tagging detectors cover the photon  
 244 energy range between 2.9 GeV and 11.4 GeV and provide  
 245 relative energy resolution of about 0.2%. The spot size of the  
 246 collimated photon beam had a diameter of about 6 mm.

247 In the beginning of the calibration run, we adjusted the PMT  
 248 high voltage for each module in order to equalize signal pulse

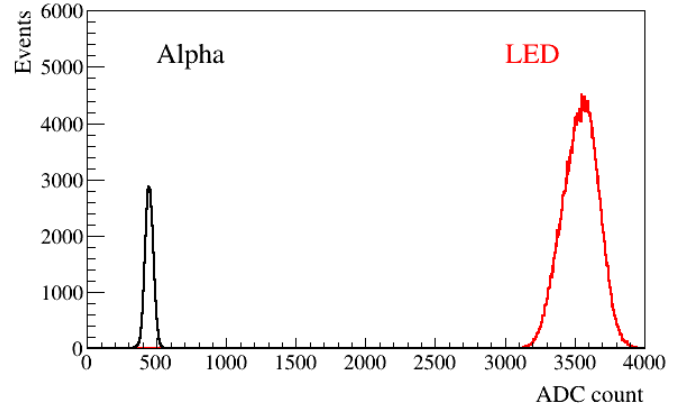


Figure 5: Flash ADC signal amplitudes induced by the LED and the  $\alpha$ -source in the reference PMT.

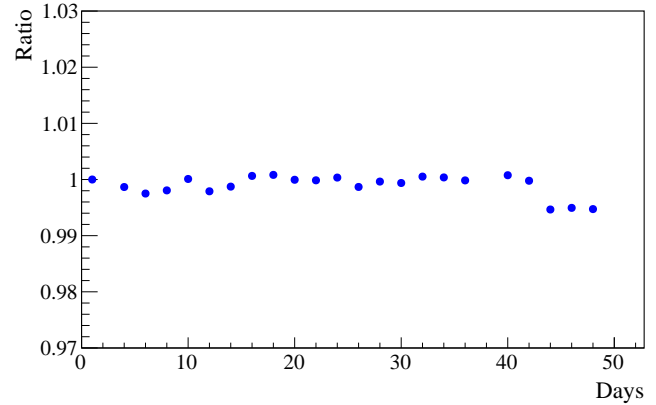


Figure 6: Ratio of signal ADC amplitudes from the LED pulser to the  $\alpha$ -source measured by the reference PMT during different run periods of the 48-day long PrimEx  $\eta$  experiment. The ratio is normalized to data in the beginning of the run.

249 amplitudes induced by 10 GeV beam photons. The amplitude  
 250 was set to 340 ADC counts. An example of flash ADC signal  
 251 amplitude in the calorimeter module as a function of the beam  
 252 energy is presented in Fig. 7. The calibration of each module  
 253 was refined by reconstructing showers in the calorimeter and  
 254 constraining the reconstructed energy to the known beam en-  
 255 ergy.

During the calibration runs, we estimated the non-uniformity  
 of the 140 CCAL modules by measuring the relative energy  
 resolution for each individual module exposed to the beam. The  
 energy resolution obtained for 6 GeV photons is presented in  
 Fig. 8. The distribution is fit to a Gaussian function. The spread  
 of the distribution is found to be smaller than 5%.

During calibration, we observed some a non-linearity of the  
 PMT active base with the large amplification factor of 24, on  
 the level of a few percent, which impacted both the pulse peak  
 and pulse integral. The base performance became linear when  
 the amplifier gain was reduced. ~~The CCAL electronics is being currently adjusted; modified active bases will be installed~~



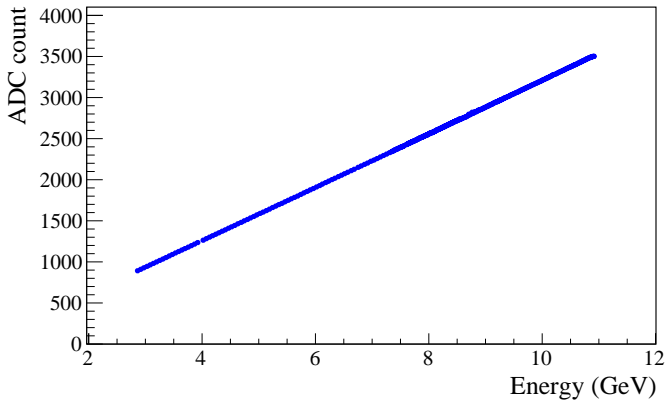


Figure 7: ADC signal pulse amplitude in the CCAL module as a function of the beam energy.

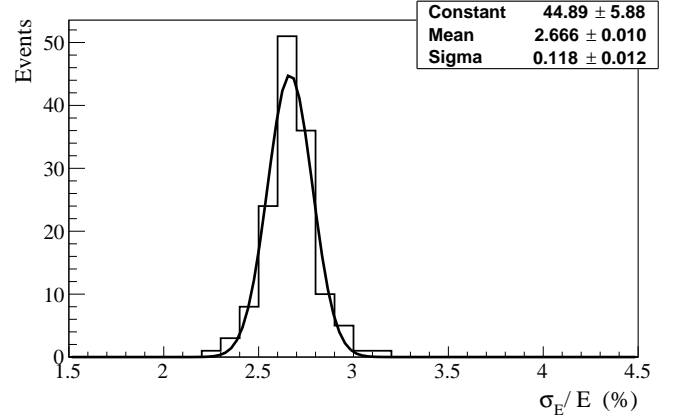


Figure 8: Relative energy resolution of 140 CCAL modules for 6 GeV beam photons.

before the new PrimEx  $\eta$  run in 2021. We subsequently replaced the original PMT active bases with the gain of 24 for 9 CCAL modules (in the array of 3x3 modules) with modified bases where the amplifier was bypassed and measured the energy resolution for different beam energies. An example of the energy deposited by 10 GeV photons incident on the center of the middle module is shown in Fig. 9. The distribution was fit to a Crystal Ball function, which was named after the Crystal Ball collaboration and was implemented in the ROOT data analysis framework [16]. The energy resolution as a function of the beam energy is shown in Fig. 10. The resolution was fit to the following function:

$$\frac{\sigma_E}{E} = \frac{S}{\sqrt{E}} \oplus \frac{N}{E} \oplus C, \quad (1)$$

where  $S$  represents the stochastic term,  $N$  the electronic noise and  $C$  the constant term,  $E$  is the beam energy in GeV, and the symbol  $\oplus$  indicates a quadratic sum. The fit yields:  $S = 2.63 \pm 0.01\%$ ,  $N = 1.07 \pm 0.09\%$ , and  $C = 0.53 \pm 0.01\%$ . The resolution was found to be about 10% better than that measured with the original base with the gain of 24. The energy resolution is consistent with that of the HyCal calorimeter [13], which was instrumented with crystals produced by SICCAS in 2001 and was used in several experiments in Jefferson Lab's experimental Hall B. The HyCal  $\text{PbWO}_4$  crystals have the same transverse size of 2.05 cm x 2.05 cm, but a smaller length of 18 cm. The CCAL calibration was fine-tuned during the PrimEx run by using showers of reconstructed Compton candidates.

### 3.6. Performance during the PrimEx run

In the PrimEx  $\eta$  experiment, we reconstruct Compton events produced by beam photons with  $E_{\text{beam}} > 6$  GeV. This energy range is covered by the pair spectrometer [17], which determines the photon flux needed for cross section measurements. In order to accept Compton events during data taking and to reduce background originating from low-energy electromagnetic and hadronic interactions, the CCAL was integrated to the Level 1 trigger system of the GlueX detector. The physics trigger was based on the total energy deposited in the forward and

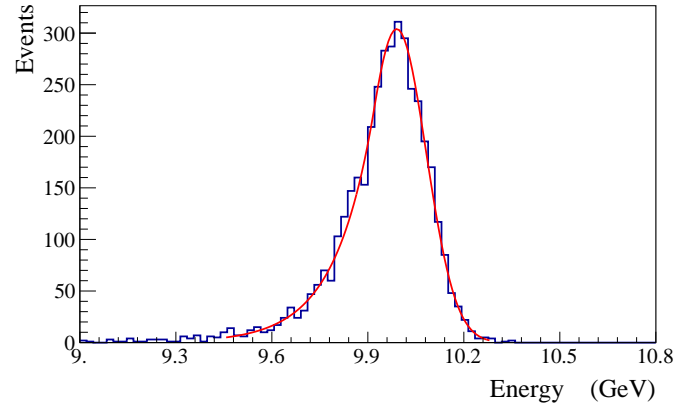


Figure 9: Energy distribution deposited by 10 GeV beam photons. The spectrum is fit to a Crystal Ball function.

Compton calorimeters. The GlueX trigger is implemented on special-purpose programmable electronics modules with FPGA chips. The trigger architecture is described in Ref. [18]. The trigger rate as a function of the energy threshold is presented in Fig. 11. We collected data using a relatively small energy threshold of 3 GeV at a trigger rate of about 18 kHz. This rate did not produce any dead time in the DAQ and trigger systems. The trigger rate was reproduced by the detailed Geant detector simulation.

The rate in the CCAL modules during the experiment is presented in Fig. 12. In this plot, the photon beam goes through the center of the hole of 2x2 modules in the middle of the detector. The rate is the largest in innermost detector layers closest to the beam line. The maximum trigger rate in the detector module was about 200 kHz for an energy threshold of 30 MeV, which is equivalent to a signal pulse amplitude of 5 mV. Before the experiment, we performed a high-rate performance study of the PMT and electronics using a laser and an LED pulser and did not find any degradation of the PMT gain in run conditions similar to the PrimEx  $\eta$  up to 3-4 MHz [19].

Timing resolution of reconstructed showers is an impor-

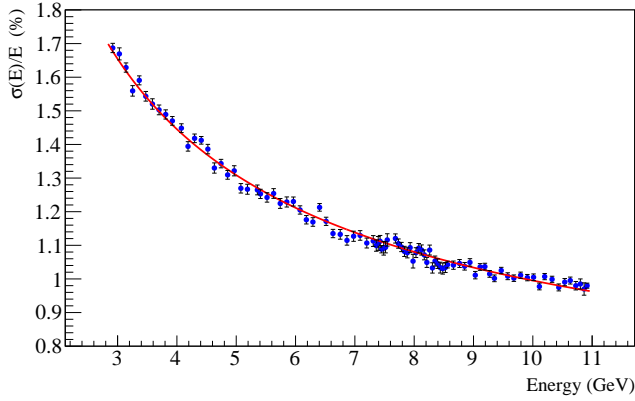


Figure 10: Energy resolution as a function of the photon energy.

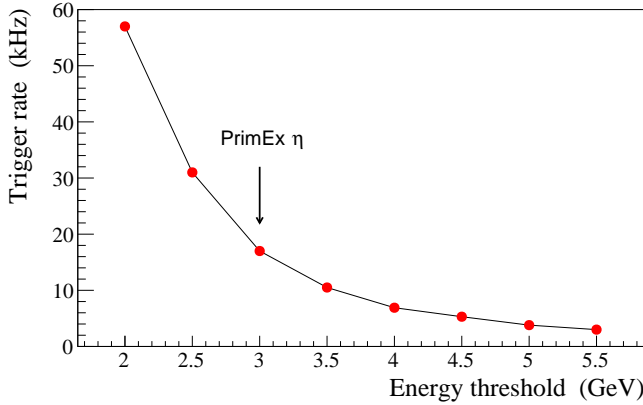


Figure 11: Trigger rate as a function of the total energy deposited in the FCAL and CCAL. The arrow indicates the energy threshold used in PrimEx  $\eta$  production runs.

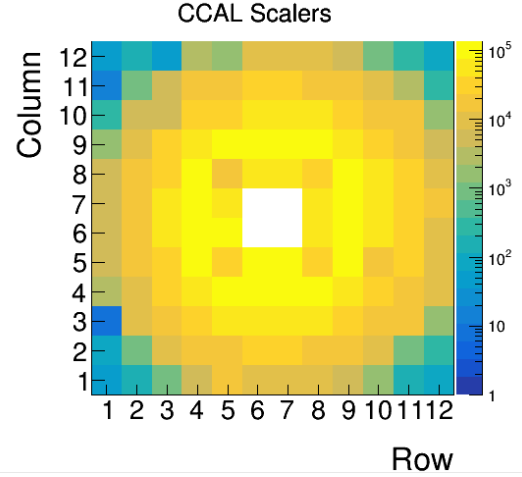


Figure 12: Rates in the CCAL modules during PrimEx  $\eta$  production run. The energy threshold corresponds to 30 MeV. The beam goes through the center of the hole in the middle of the plot (plot will be updated).

ps for 1 GeV and 9 GeV showers, respectively. In the PrimEx experiment, CCAL allowed a clear separation of beam photons originating from different beam bunches.

An electron and photon produced in the Compton scattering process were detected by reconstructing two showers, one in the FCAL and another one in CCAL. The event topology of the reaction is such that the more energetic electron predominantly goes into the Compton calorimeter, while the photon strikes the FCAL. Reconstruction of electromagnetic showers in the FCAL is performed using an algorithm described in Ref. [20], which is a part of the standard GlueX reconstruction software. For the CCAL, we implemented an algorithm originally developed for the GAMS spectrometer [21], which was later adopted for the HyCal [13] in JLab's experimental Hall B. The algorithm provides a good separation of overlapping showers in the calorimeter by using profiles of electromagnetic showers. The elasticity distribution, defined as the reconstructed energy in the event minus the beam energy, is presented in Fig. 14 for Compton candidates produced by beam photons in the energy range between 6 GeV and 7 GeV. The solid line shows the fit of this distribution to the sum of a Gaussian and a second order polynomial function. The energy resolution of reconstructed Compton candidates is about 130 MeV. In this plot, we subtracted background originating from multiple beam photon candidates in the event due to accidental hits in the GlueX tagging detectors. The background was measured using off-time interactions and amounted to about 15%. The relatively small background, on the level of 10%, produced by interactions of beam photons with the beamline material downstream the GlueX target was measured using empty-target runs and was excluded from Fig. 14. The CCAL allowed to clearly reconstruct Compton events in the PrimEx  $\eta$  experiment.

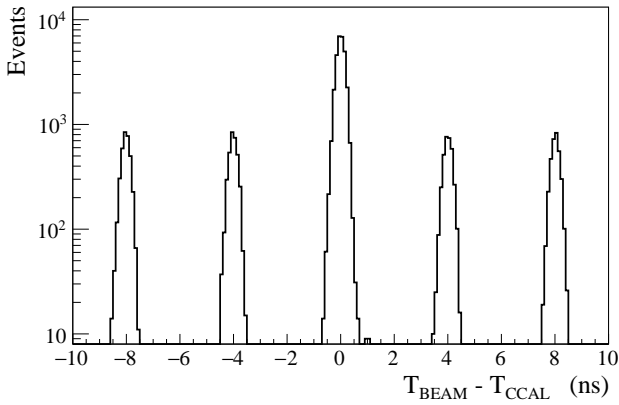


Figure 13: Time difference between beam photons and reconstructed CCAL showers for Compton candidates. Peaks are separated by the beam bunch period of 4 ns.

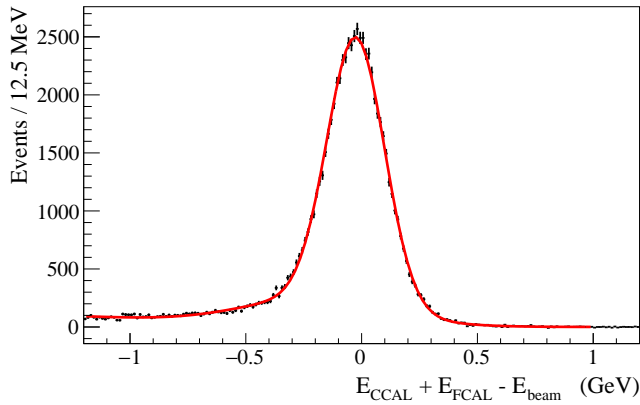


Figure 14: Elasticity distribution of reconstructed Compton candidates.

#### 4. Upgrade of the GlueX forward calorimeter

The forward calorimeter of the GlueX detector consists of 2800 lead glass modules, with a size of 4 cm x 4 cm x 45 cm, and is positioned about 6 m downstream of the target, as shown in Fig. 1. The FCAL covers a polar angle of photons produced from the target between 1° and 11° and detects showers with energies in the range of 0.1 - 8 GeV. The Cherenkov light produced in the module is detected by FEU-84-3 photomultiplier tubes produced in Russia, instrumented with Cockcroft-Walton bases [22]. The typical energy resolution of the FCAL is  $\sigma_E/E = 6.2\%/\sqrt{E} \oplus 4.7\%$ .

The future physics program with the GlueX detector in Hall D will require an upgrade of the inner part of the forward calorimeter with high-granularity, high-resolution PbWO<sub>4</sub> crystals. The lead tungstate insert will improve the separation of clusters in the forward direction and the energy resolution of reconstructed photons by about a factor of two. Lead tungstate crystals possess better radiation hardness compared to lead glass, which is important for the long term operation of the detector at high luminosity. We propose to build a 1 m x 1 m

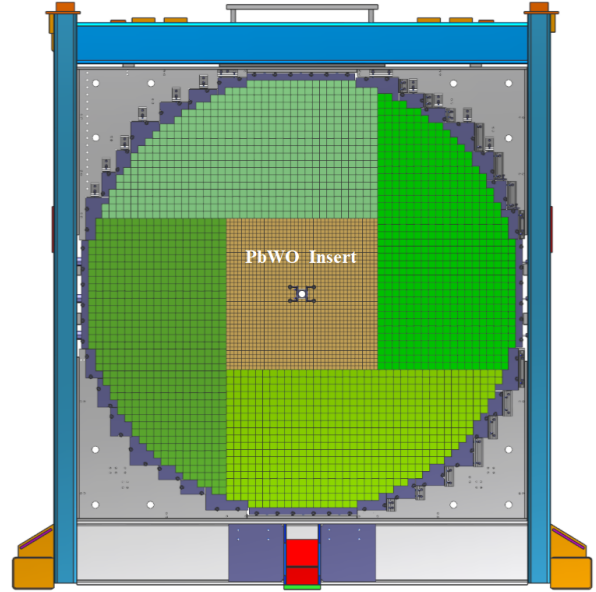


Figure 15: FCAL frame with calorimeter modules installed: PbWO<sub>4</sub> crystals (brown area), lead glass blocks (green). The photon beam passes through the hole in the middle of the calorimeter.

insert, which will require about 2496 modules. Similar to the CCAL, the insert will have a beam hole of 2 x 2 modules and a tungsten absorber used to cover the detector layer closest to the beamline. A schematic view of the FCAL frame with the installed lead tungstate insert is presented in Fig. 15. Due to the different size of the lead glass bars and lead tungstate crystals, the lead glass modules stacked around the PbWO<sub>4</sub> insert will form four regions with a relative offset between modules; those regions are shown in green color in this plot.

The PbWO<sub>4</sub> module design of the FCAL insert will essentially be the same as for the CCAL, except for some small modifications needed to handle the magnetic field present in the FCAL region. The PMT housing made of the G-10 fiberglass material will be replaced by iron housing in order to reduce the magnetic field. The housing length will be increased to extended the magnetic shield beyond the PMT photo cathode. An acrylic optical light guide will be inserted inside the PMT housing to couple the crystal and PMT.

The upgraded FCAL will be operated in GlueX experiments using a 30 cm long liquid hydrogen target at the designed photon flux of  $5 \cdot 10^7 \gamma/\text{sec}$  in the energy range between 8 GeV and 9 GeV. The designed luminosity is significantly larger than that used in the PrimEx  $\eta$  experiment and was achieved after the PrimEx run in the fall of 2019. In order to finalize the design of the PMT electronics, it is important to understand detector rates in the FCAL insert, especially in layers close to the beamline. We used CCAL during high-intensity GlueX runs to study run conditions for the FCAL insert.

##### 4.0.1. PMT magnetic shield

The longitudinal (directed along the beamline) and transverse (directed perpendicular to the axis of of the beamline) compo-

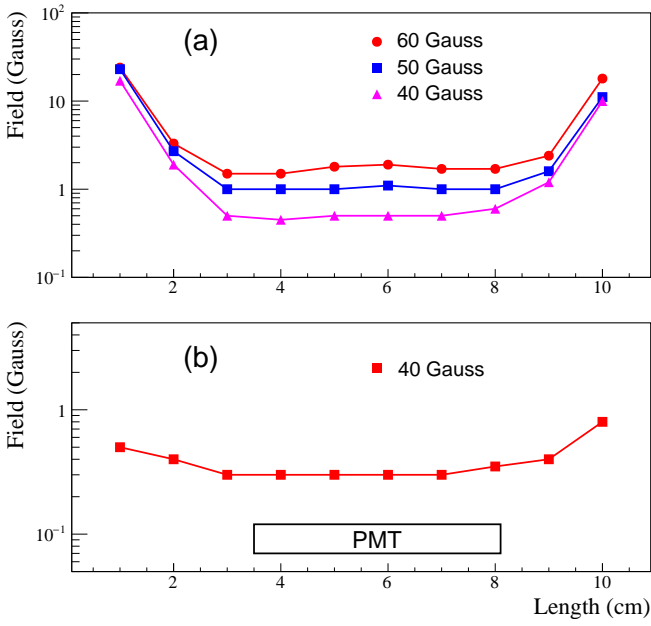


Figure 16: Magnetic field distribution inside the PMT shield housing as a function of the distance from the housing face. Plot (a) corresponds to the longitudinal field and plot (b) corresponds to the transverse field. Markers denote different field values produced by the Helmholtz coils.

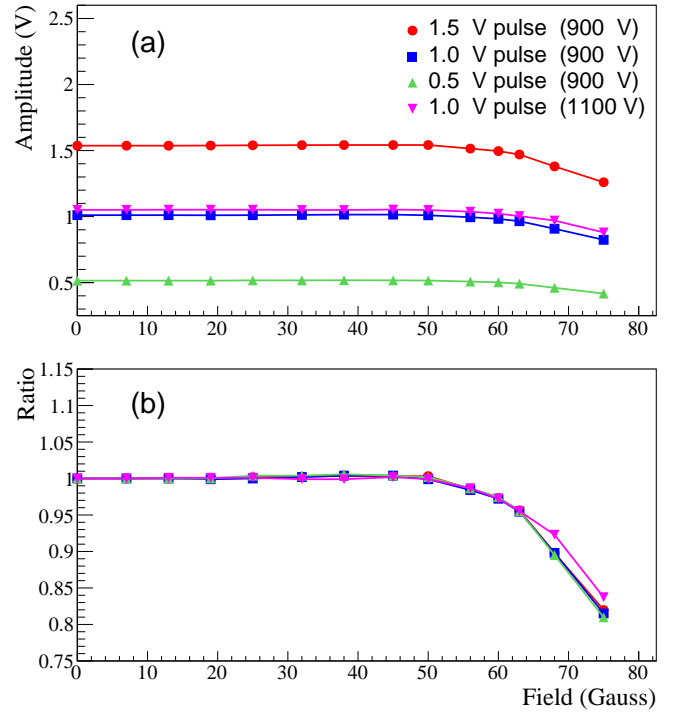


Figure 17: Signal amplitudes of shielded PMT induced by an LED as a function of the magnetic field (a). Amplitudes, normalized to measurements without magnetic field (b). The PMT response was measured for different intensities of light pulse and HV settings as shown by different polymarkers.

nents of the magnetic field produced by the GlueX solenoid magnet in the FCAL PbWO<sub>4</sub> insert area vary between 40 - 50 Gauss and 0 - 8 Gauss, respectively. The longitudinal field is the largest on the beamline, where the transverse component is practically absent. We studied the PMT magnetic shielding using a prototype consisting of an array of 3x3 PMT iron housings made of AISI 1020 steel, which was positioned in the middle of Helmholtz coils. Each housing had a size of 20.6 mm x 20.6 mm x 100 mm with a 19.9 mm round hole in the middle for the PMT. This corresponds to the realistic size of the magnetic shield that will be used in the calorimeter module assembly. Inside the housing we inserted two layers of  $\mu$ -metal Co-Netic cylinders, with thicknesses of 350  $\mu$ m and 50  $\mu$ m, separated from each other by a Mylar film. The thickest cylinder was spot welded and annealed.

The Helmholtz coils had a diameter of about 1 m and can generate a uniform magnetic field with variable strength below 100 Gauss. A Hall probe was inserted into the central module of the prototype to measure the magnetic field at different Z-positions along the length of the cylinder. The field was measured for two different orientations of the prototype with respect to the magnetic field: field oriented along the PMT (longitudinal,  $B_z$ ) and perpendicular to the PMT housing (transverse,  $B_x$ ). Field measurements are presented in Fig. 16. The PMT shield significantly reduce both the longitudinal and transverse fields to the level of  $B_z \sim 1$  Gauss and  $B_x \ll 1$  Gauss. The transverse field, which is well shielded, is more critical for the PMT operation, as it is directed perpendicular to the electron trajectory inside the photo tube and deflects electrons, resulting in the degradation of the photon detector efficiency and gain. The

field reaches a plateau at  $Z = 3$  cm from the face of the housing. We will use 3.5 cm long acrylic light guides, in order to place the most sensitive to the magnetic field area of the PMT between the photocathode and the last dynode (4.6 cm long) in the region with the smallest magnetic field, as shown in Fig. 16.

We studied the performance of the shielded PMT in the magnetic field using an LED pulser. A blue LED with a light diffuser was placed about 20 cm from the PMT housing prototype and was aligned with the middle module. The PMT response was measured for different pulse amplitudes and operational high voltage. In order to study the contributions from longitudinal and transverse field components we rotated the prototype by different angles. Signal amplitudes as a function of the magnetic field measured in the prototype tilted by about 10 degrees are presented on the left plot of Fig. 17. Amplitudes, normalized to measurements without magnetic field, are shown on the bottom plot. The relative degradation of the signal amplitude for the maximum field in the FCAL insert region of  $B = 50$  Gauss ( $B_z = 49$  Gauss and  $B_x = 8.6$  Gauss) was measured to be less than 1%.

#### 4.0.2. Light guide studies

Studies of the magnetic shielding demonstrated that the PMT has to be positioned inside the iron housing and Co-Netic  $\mu$ -metal cylinder at the distance of at least 3 cm from the face of the PbWO<sub>4</sub> crystal. In the FCAL insert module, we decided to



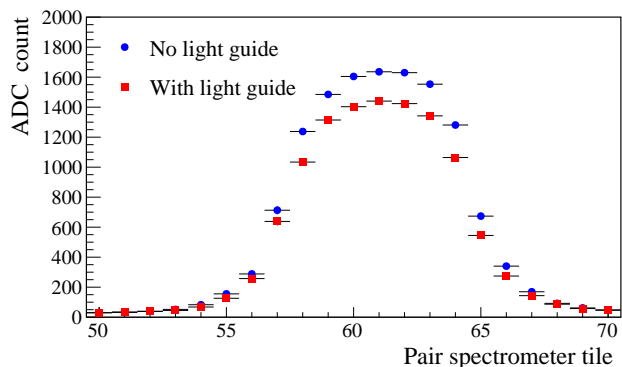


Figure 18: ADC amplitudes of the calorimeter module as a function of the pair spectrometer tile for two configurations: the PMT directly coupled to the PbWO<sub>4</sub> crystal (circles), and the PMT coupled to the module using an optical light guide (boxes).

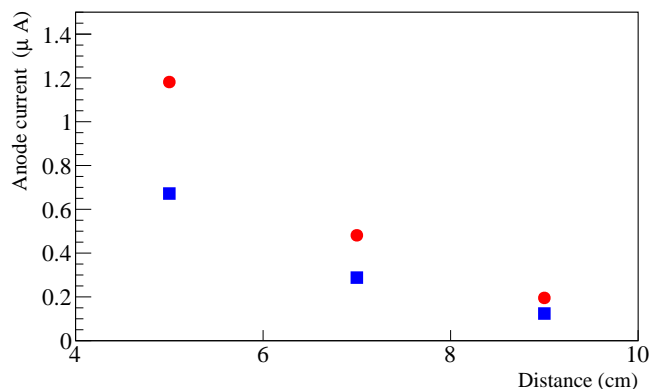


Figure 19: Typical PMT anode current of CCAL modules positioned at different distances from the beamline. Circles correspond to the nominal GlueX luminosity, boxes correspond to 60% of the nominal luminosity.

use a 3.5 cm long acrylic cylindrical light guide with a diameter of 18.5 mm between the PMT and the crystal. The light guide is wrapped with reflective ESR foil. The light guide is attached to the PMT with Dymax 3094 UV curing glue. Optical coupling to the crystal is provided by a “silicon cookie”: a 1 mm thick transparent rubber cylinder made of the room temperature vulcanized silicon compound, RTV615. This type of material has a widespread application in photodetectors and simplifies the module design. The silicon cookie is not glued to the light guide and the crystal, so the module can be easily disassembled if its PMT needs to be replaced.

We compared light losses of the FCAL insert module instrumented with the light guide with the CCAL module, where the PMT was coupled directly to the crystal using an optical grease. Light collection was measured using electrons provided by the Hall D pair spectrometer (PS) [17]. The PS is used to measure the flux of beam photons delivered to the experimental hall by detecting electromagnetic electron-positron pairs produced by the photons in a thin converter inserted to the beam. Leptons from the pair are deflected in a dipole magnet and detected using two scintillator detectors placed in the electron and positron arms of the spectrometer. Each detector consists of 145 tiles which cover the energy range of leptons between 3 GeV and 6 GeV.

We first positioned the CCAL module behind the PS and measured ADC amplitudes of signal pulses induced by electrons with the energy of about 4 GeV. The module was subsequently modified by adding the light guide to the same PMT and crystal and was placed to the same spot of the PS test setup. Results of the measurements are presented Fig. 18. On this plot the ADC amplitude of the calorimeter module is presented as a function of the PS tile for the two module configurations with and without the light guide. The light guide results in a relatively small loss of light of about 15% compared with the CCAL module. We note that wrapping the light guide with the reflective material is important. Losses in unwrapped light guide constitute about 35%. We repeated light collection mea-

surements using two more modules and obtained consistent results.

#### 4.0.3. Detector rate

The PMT anode current is one of the critical characteristics that have to be considered during the design of the PMT divider. Typically the anode current should be on the level of a few micro amperes and significantly smaller than the divider current in order to provide stable performance of the PMT base and prevent the long-term degradation of the PMT. The anode current was measured using a special random trigger, which was used to read out flash ADC raw data for each CCAL channel in a time window of 400 ns. The window size corresponds to 100 flash ADC samples. The average ADC voltage in the readout window was determined by summing up amplitudes in the readout window and normalizing them to the window size. The anode current can be related to the average ADC voltage as

$$I = \frac{\bar{A}}{R} \cdot \frac{1}{G}, \quad (2)$$

where  $\bar{A}$  is the ADC voltage in units of Volts,  $R$  is the input impedance of the amplifier ( $\sim 50 \Omega$ ), and  $G$  is the amplifier gain of 24. The typical anode current measured in CCAL modules situated at different distances from the beam line is presented in Fig. 19. Modules from the first CCAL layer closest to the beamline and the outer most layer were not used in the analysis. These modules were covered by a Tungsten absorber and obscured by the FCAL. The rate in the detector is dominated by the forward-directed electromagnetic background. The anode current is the largest in the innermost layer of the detector closest to the beam line and amounts to about 1.4  $\mu\text{A}$ . This current can be compared to the PMT divider current of 300  $\mu\text{A}$ . The CCAL measurements can be used to estimate anode current in the FCAL lead tungstate insert. The largest PMT current in the PbWO<sub>4</sub> module closest to the beam line is conservatively estimated to be about 20  $\mu\text{A}$  for a PMT base operated at 1 kV, and assuming that no amplifier is used. The detector rate drops

555 rapidly with the increase of the radial distance from the beam-607  
556 line. We are considering to instrument PMTs in a few inner608  
557 layers with an amplifier with a gain of 5 and to omit the ampli-609  
558 fier on other modules. 610

## 5. Neutral Particle Spectrometer 611

560 The NPS is a new facility in Hall C that will allow access to614  
561 precision small cross section measurements with neutral final615  
562 states. The NPS consists of an electromagnetic calorimeter pre-616  
563 ceded by a sweeping magnet. As operated in Hall C, it replaces617  
564 one of the focusing spectrometers. 618

565 The NPS science program currently features six fully ap-619  
566 proved experiments. E12-13-010 [4] and E12-06-114 [5] ex-620  
567 periments will measure the Exclusive Deeply Virtual Comp-621  
568 ton Scattering and  $\pi^0$  cross sections to the highest  $Q^2$  acces-622  
569 sible at Jefferson Lab. Both experiments will provide im-623  
570 portant information for understanding Generalized Parton Dis-624  
571 tributions (GPD). The E12-13-007 [6] experiment will study625  
572 semi-inclusive  $\pi^0$  electroproduction process and seeks to vali-626  
573 date the factorization framework that is needed by the entire 12627  
574 GeV Jefferson Lab semi-inclusive deep-inelastic scattering pro-628  
575 gram. Measurements of Wide-Angle and Timelike Compton629  
576 Scattering reactions will be performed by the E12-14-003 [7]630  
577 and E12-17-008 [8] experiments. These measurements will631  
578 allow to test universality of GPDs using high-energy photon632  
579 beams. The NPS will also be used in the E12-14-005 [9] exper-633  
580 iment to study exclusive production of  $\pi^0$  at large momentum634  
581 transfers in the process  $\gamma p \rightarrow \pi^0 p$ . Hard exclusive reactions635  
582 provide a testing ground for quantum chromodynamics at inter-636  
583 mediate energies. 637

584 The NPS science program requires neutral particle detection638  
585 over an angular range between 6 and 57.3 degrees at distances639  
586 of between 3 and 11 meters <sup>1</sup> from the experimental target. The  
587 experiments will use a high-intensity beam of electrons with  
588 the energies of 6.6, 8.8, and 11 GeV, and a typical luminosity  
589 of  $\sim 10^{38}$  cm<sup>-2</sup>s<sup>-1</sup> as well as a secondary beam of photons  
590 incident on a liquid hydrogen target. A vertical-bend sweeping  
591 magnet with integrated field strength of 0.3 Tm will be installed,  
592 in front of the spectrometer in order to suppress and eliminate  
593 background of charged particle tracks originating from the tar-  
594 get. The photon detection is the limiting factor of the exper-  
595 iments. Exclusivity of the reaction is ensured by the missing-  
596 mass technique and the missing-mass resolution is dominated  
597 by the energy resolution of the calorimeter. The calorimeter  
598 should provide the spatial resolution of 2-3 mm and the energy  
599 resolution of about  $2\%/\sqrt{E}$ . 649

600 The NPS consists of 1080 PbWO<sub>4</sub> crystals which form an  
601 array of 30x36 modules, ~~where the outer layers only have to~~  
602 ~~catch the showers~~. Similarly to the FCAL insert in Hall D, the  
603 NPS will be built from the crystals of the same size, and in-  
604 strumented with the same PMTs and readout electronics. Each  
605 crystal will be wrapped with the reflective ESR foil and posi-  
606 tioned inside the support structure, where the modules will be

separated from each other by thin carbon fiber plates. The de-  
tector will be positioned inside the temperature-controlled box  
on a movable platform. The details of the mechanical assembly  
and commissioning of the NPS are currently under development  
and is the subject of a forthcoming publication.

The maximum rate in the calorimeter of the NPS experi-  
ments will be maintained on the level below 1 MHz per mod-  
ule. Based on Monte Carlo simulation, the integrated doses for  
the E12-13-010 experiment are 1.7 MRad at the center and 3.4  
MRad at the edges of the calorimeter and the maximum antic-  
ipated dose rate is on the level of a kRad/hour. The integrated  
doses for the other experiments do not exceed  $< 500$  kRad<sup>2</sup>.  
The detector will be instrumented with the light monitoring sys-  
tem. Light from blue LED will be distributed to each calorime-  
ter module through a quartz optical fiber, attached to the crystal  
from the PMT side. The LED system will be used for calibra-  
tion and allow to cure crystals whose performance is degraded  
due to radiation. Signal pulses from the PMT will be digitized  
using flash ADCs hosted in VXS crates. Energy deposition in  
the calorimeter, will be used in the trigger system of the exper-  
iments. Integration of the detector to the trigger will be per-  
formed by means of the trigger electronics modules designed at  
Jefferson Lab.

Radiation hardness and good optical quality of lead tungstate  
crystals are critical for the NPS calorimeter. The NPS collab-  
oration, in a synergistic effort with the EIC eRD1 consortium,  
has characterized to date over 1200 PbWO<sub>4</sub> crystals produced  
by CRYTUR and SICCAS from 2014 to present. The results of  
these studies have been published in Ref. [10]. CRYTUR crys-  
tal samples were found to have greater overall uniformity in  
transmittance, light yield, and better radiation hardness. Of the  
samples characterized by the NPS collaboration 140 SICCAS  
crystals have been used in the CCAL detector.

## 6. Summary

We described the design and performance of the Compton  
calorimeter, which was constructed using 140 lead tungstate  
PbWO<sub>4</sub> crystals recently produced by SICCAS. The calorime-  
ter was successfully used in the PrimEx  $\eta$  experiment in spring  
of 2019 for reconstruction of Compton scattering events. The  
CCAL served as a prototype for two large-scale electromag-  
netic calorimeters based on the PbWO<sub>4</sub> crystals: the lead  
tungstate insert of the forward calorimeter of the GlueX detec-  
tor and the neutral particle spectrometer. Experience gained  
during construction and operation of the CCAL provided im-  
portant information for finalizing the design of FCAL PbWO<sub>4</sub>  
modules and PMT dividers and also served to further optimize  
the NPS calorimeter. We presented the design of the FCAL lead  
tungstate insert and gave an overview of the NPS project.

<sup>2</sup>The radiation doses are larger than that for the FCAL lead tungstate insert,  
where the integrated dose for modules positioned closest to the beamline is  
smaller than 200 kRad.

<sup>1</sup>the minimum NPS angle at 3m is 8.5 degrees, at 4m it is 6 degrees



655 **7. Acknowledgments**

656 This work was supported by the Department of Energy. Jef-  
657 ferson Science Associates, LLC operated Thomas Jefferson  
658 National Accelerator Facility for the United States Depart-  
659 ment of Energy under contract DE-AC05-06OR23177. This  
660 work was supported in part by NSF grants PHY1714133 and  
661 PHY2012430. We thank the NPS collaboration/project for pro-  
662 viding PbWO<sub>4</sub> crystals and PMTs used in the construction of  
663 the CCAL.

664 **References**

- 665 [1] S. Adhikari, *et al.*, Nucl. Instrum. Meth. A **987**, 164807 (2021).  
666 [2] JLab Experiment **E12-12-002A**: Eta Decays with Emphasis on Rare Neu-  
667 tral Modes:The JLab Eta Factory (JEF) Experiment, [https://www.  
668 jlab.org/exp\\_prog/proposals/14/PR12-14-004.pdf](https://www.jlab.org/exp_prog/proposals/14/PR12-14-004.pdf).  
669 [3] T. Horn, J. Phys. Conf. Ser. **587** (2015) no.1, 012048.  
670 [4] JLab experiment **E12-13-010**: Exclusive Deeply Virtual Compton and  
671 Neutral Pion Cross-Section Measurements in Hall C, [https://www.  
672 jlab.org/exp\\_prog/proposals/13/PR12-13-010.pdf](https://www.jlab.org/exp_prog/proposals/13/PR12-13-010.pdf).  
673 [5] JLab experiment **E12-06-114**: Measurements of the Electron-Helicity  
674 Dependent Cross Sections of Deeply Virtual Compton Scattering with  
675 CEBAF at 12 GeV, [https://www.jlab.org/exp\\_prog/proposals/  
676 06/PR12-06-114.pdf](https://www.jlab.org/exp_prog/proposals/06/PR12-06-114.pdf).  
677 [6] JLab experiment **E12-13-007**: Measurement of SemiInclusive  $\pi^0$  Pro-  
678 duction as Validation of Factorization, [https://www.jlab.org/exp\\_  
679 prog/proposals/13/PR12-13-007.pdf](https://www.jlab.org/exp_prog/proposals/13/PR12-13-007.pdf).  
680 [7] JLab experiment **E12-14-003**: Wide-angle Compton Scattering at 8  
681 and 10 GeV Photon Energies, [https://www.jlab.org/exp\\_prog/  
682 proposals/14/PR12-14-003.pdf](https://www.jlab.org/exp_prog/proposals/14/PR12-14-003.pdf).  
683 [8] JLab experiment **E12-17-008**: Polarization Observables in Wide-Angle  
684 Compton Scattering at large  $s$ ,  $t$ , and  $u$ , [https://www.jlab.org/exp\\_  
685 prog/proposals/17/PR12-17-008.pdf](https://www.jlab.org/exp_prog/proposals/17/PR12-17-008.pdf).  
686 [9] JLab experiment **E12-14-005**: Wide Angle, Exclusive Photoproduction  
687 of  $\pi^0$  Mesons, [https://www.jlab.org/exp\\_prog/proposals/14/  
688 PR12-14-005.pdf](https://www.jlab.org/exp_prog/proposals/14/PR12-14-005.pdf).  
689 [10] T. Horn, *et al.*, Nucl. Instrum. Meth. A **956**, 163375 (2020).  
690 [11] Electron-Ion collider user group yellow report, [http://www.eicug.  
691 org/web/content/detector-rd](http://www.eicug.org/web/content/detector-rd).  
692 [12] JLab Experiment **E12-10-011**, A Precision Measurement of the  $\eta$  Ra-  
693 diative Decay Width via the Primakoff Effect, [https://www.jlab.org/  
694 exp\\_prog/proposals/10/PR12-10-011.pdf](https://www.jlab.org/exp_prog/proposals/10/PR12-10-011.pdf).  
695 [13] M. Kubantsev *et al.*, AIP Conf. Proc. **867**, no.1, 51-58 (2006). A. Gaspar-  
696 ian, Proceedings of the 11th International Conference on Calorimetry in  
697 High-Energy Physics, 109-115 (2004).  
698 [14] V. Popov and H. Mkrtychyan *et al.*, Proceedings of the IEEE conference,  
699 California, 2012.  
700 [15] F. Barbosa *et al.*, Proceedings of IEEE Nuclear Science Symposium,  
701 Hawaii, USA (2007).  
702 [16] R. Brun and F. Rademakers, Nucl. Instrum. Meth. A **389** (1997), 81-86.  
703 [17] F. Barbosa, *et al.*, Nucl. Instrum. Meth. A **795**, 376-380 (2015).  
704 [18] A. Somov, AIP Conf. Proc. **1560**, no.1, 700-702 (2013).  
705 [19] F. Barbosa, *et al.*, "Characterization of the NPS and CCAL readout,"  
706 GlueX-doc-3272, Jefferson Lab, (2017), [https://halldweb.jlab.  
707 org/doc-public/DocDB/ShowDocument?docid=3272](https://halldweb.jlab.org/doc-public/DocDB/ShowDocument?docid=3272).  
708 [20] R. Jones, *et al.*, Nucl. Instrum. Meth. A **566**, 366374, (2006).  
709 [21] A. Lednev, Preprint IHEP 93-153, Protvino (1993). F. Binon, *et al.*, Nucl.  
710 Instrum. Meth. A **248**, (1986).  
711 [22] A. Brunner, *et al.*, *et al.*, Nucl.Instrum. Meth. A **414** (1998).